Korean J. Chem. Eng., 40(7), 1549-1562 (2023)
DOI: 10.1007/s11814-023-1444-9
pISSN: 0256-1115
eISSN: 1975-7220

INVITED REVIEW PAPER

Current progress of electrocatalysts for anion exchange membrane fuel cells

Subin Park*,‡, Daeil Choi*,‡, Dong Wook Lee*,‡, Baeck B. Choi**, and Sung Jong Yoo*,**,***,†**

*Hydrogen Fuel Cell Research Center, Korea Institute of Science and Technology (KIST), 5 Hwarang-ro 14-gil, Seongbuk-gu, Seoul 02792, Korea
**Division of Energy & Environmental Technology, KIST School, University of Science and Technology (UST), Daejeon 34113, Korea
***KHU-KIST Department of Converging Science and Technology, Kyung Hee University, Seoul 02447, Korea
****Energy and Environment Laboratory, Korea Electric Power Corp. Research Institute, Daejeon 34056, Korea
(*Received 19 July 2022 • Revised 9 December 2022 • Accepted 31 January 2023*)

Abstract−The transition from a carbon-centered economy to an era of renewable energy has led to global attention on hydrogen energy, ultimately leading to the development of fuel cells using hydrogen as a fuel. In response to global demand, overall fuel cell technology has grown remarkably over the past few years; yet, commercialization remains sluggish owing to cost. As the cathode of a proton exchange membrane fuel cell (PEMFC), which is the most commercialized fuel cell, is markedly dependent on platinum (Pt), anion exchange membrane fuel cells (AEMFCs), which can utilize non-precious materials as cathode catalysts, have emerged as a promising alternative. Earth-abundant metals are used as cathode catalysts, and metal-free materials are used to achieve comparable performance to Pt. Compared to the single-cell performance of Pt catalysts, a gap still exists; however, the applicability of non-noble metals has been extensively evaluated. If catalyst development is accompanied by efficient electrode structure design, a significant part of the cost problem can be overcome. AEMFCs have advantages in the ORR of cathodes compared to PEMFCs; however, the HOR kinetics are quite sluggish. Therefore, the design of HOR catalysts requires another approach, not only to enhance their intrinsic activity, but also consider the poisoning induced by the use of ionomers besides PEMFCs. Therefore, a strategy based on the HOR pathway is required to lower the barrier of the rate-determining step. In this review, catalysts for AEMFCs were introduced based on their classification, and information on recent trends and issues related to catalysts was presented.

Keywords: Anion Exchange Membrane Fuel Cells (AEMFCs), Electrocatalyst, Oxygen Reduction Reaction (ORR), Hydrogen Oxidation Reaction (HOR)

INTRODUCTION

Owing to global decarbonization, the demand for clean and sustainable energy sources has increased for the next generation. Of the many potential energy sources, hydrogen has been highlighted as an energy carrier as it is not only an abundant and clean energy source, but is also not regionally dependent, such as fossil fuels [1,2]. Fuel cells are energy conversion devices that use the chemical energy of hydrogen and can directly produce electrical energy without additional mechanical processes [3-6]. Among the various fuel cells, proton exchange membrane fuel cells (PEMFCs) have been intensively assessed for decades and are the closest to commercialization, yet practical issues remain [5-8]. In particular, the sluggish oxygen reduction reaction (ORR) at the cathode lowers the overall performance of PEMFCs, which requires the use of large amounts of platinum (Pt) electrocatalysts to improve the performance [7-11]. Although non-precious metal-based electrocatalysts have been reported for the ORR, they are insufficient to completely replace Pt-based electrocatalysts, especially in terms of stability in acidic environments [12-17]. The electrode accounts for a significant portion (~50%) of the fuel cell stack cost [18-20], and its cost is generally determined by the amount of catalyst used. The cost issue caused by the dependence on Pt hinders the wide dissemination of PEMFCs; therefore, research on catalyst development with reduced amounts of Pt usage or the replacement of the Pt-group metal with cheap materials is required to accelerate commercialization. Anion exchange membrane fuel cells (AEMFCs) have garnered attention as an alternative to PEMFCs owing to the availability of non-precious materials as electrocatalysts at the cathode [21-23]. The alkaline environment is more favorable than an acidic environment from the viewpoint of ORR kinetics, enabling the use of non-precious-material-based electrocatalysts [21]. In contrast to alkaline ORR kinetics, hydrogen oxidation reaction (HOR) kinetics in alkaline environments is intrinsically two orders of magnitude lower than that of acid, causing the anode to be dependent on Pt-based electrocatalysts [24-27]. Despite the unfavorable HOR in alkaline electrolytes, research on HOR catalysts is insufficient compared to the progress of ORR catalysts. Alkaline HOR catalysts are conventionally categorized into Pt-group metal (PGM)-based and PGM-free catalysts as shown in Fig. 1 [24]. Studies with high HOR performance using PGM-based catalysts while reducing the amount

†To whom correspondence should be addressed.
E-mail: ysj@kist.re.kr
‡These authors equally contributed to this work.

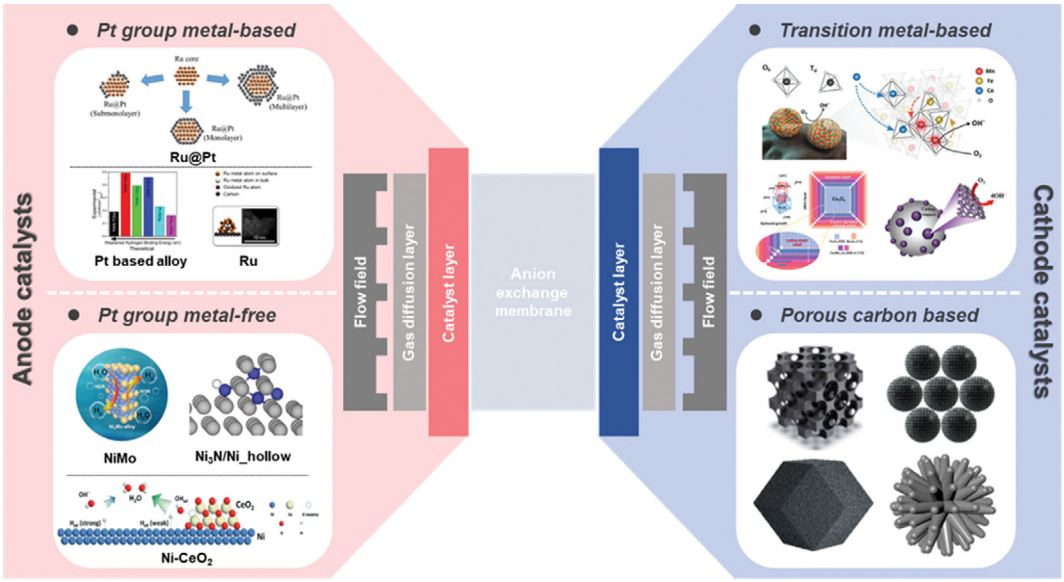

Fig. 1. Schematic diagram presenting classification of electrocatalysts for AEMFC.

of PGM were performed by controlling the composition and/or structure of the nanocatalysts [28-32]. Further, Ni-based catalysts have been reported as PGM-free catalysts [33-38]. In the design of anode catalysts, not only their HOR activity, but also their resistance to poisoning should be considered, as pure hydrogen may not be supplied depending on the hydrogen supply [39,40]. When hydrogen is supplied via alcohol oxidation, CO is produced as an intermediate [40]. As Pt is particularly susceptible to CO adsorption, research is required to develop catalysts that can withstand CO poisoning [41-43]. Unlike the catalysts in PEMFCs, the anode catalysts in AEMFCs have an alkali cation adsorption issue due to the use of alkaline exchange ionomers containing bulky and/or phenyl group-based cations [44-47]. Therefore, a catalyst that can satisfy the HOR activity and resistance of anode catalysts in alkaline media is required. On the other hand, alkaline ORR is advantageous relative to acid ORR; however, alkaline ORR exhibits a higher overpotential and poor kinetics relative to the anode HOR owing to the higher number of electrons involved. To date, although Pt-based catalysts dominate the AEMFC cathode, numerous studies have recently been conducted on non-precious-material-based electrocatalysts, such as transition metal- and carbon-based materials (Fig. 1) with ORR activity and durability comparable to those of Pt-based catalysts [21,23,48-52]. The availability of non-noble metals as alkaline cathode catalysts is attributed to a different mechanism from that in acid. In alkaline environments, the adsorbed OH facilitates the electron transfer pathway in the outer sphere, which induces non-specificity that not only allows Pt, but also non-precious materials as catalysts [23]. This review elucidates strategies for designing efficient catalysts beyond comprehensive information on the trends of the latest developed catalysts based on HOR and ORR mechanisms in AEMFCs.

HOR IN ALKALINE ENVIRONMENTS

Typically, alkaline HOR proceeds through the following elementary steps:

$$\text{Total HOR: } H_2+2OH^- \rightarrow 2H_2O+2e^- \quad (1)$$

$$\text{Tafel: } H_2+2* \rightarrow 2H_{ad} \quad (2)$$

$$\text{Heyrovsky: } H_2+OH^-+* \rightarrow H_{ad}+H_2O+e^- \quad (3)$$

$$\text{Volmer: } H_{ad}+OH^- \rightarrow H_2O+e^-+* \quad (4)$$

where * denotes surface sites with a high affinity for H atoms and H_{ad} is the adsorbed hydrogen. In the Tafel step, H_2 is adsorbed onto the metal surface without electron transfer, whereas in the Heyrovsky step, H_2 dissociative adsorption occurs with the assistance of neighboring OH^- with electron transfer from H_2 to the catalytically active site. Subsequently, the absorbed H_{ad} reacts with OH^- to form water and release electrons, as indicated by the Volmer step (Fig. 2(a)). Several theories have been proposed for the evaluation of the HOR, with hydrogen bonding energy (HBE) theory and bifunctional theory as two widely used theories for predicting the performance of HOR catalysts (Fig. 2(b)).

HOR occurs at the catalytic active site through several steps, including dissociation, adsorption, and desorption of H_2 molecules along the Tafel/Heyrovsky-Volmer pathway [24,25,53-62]. Therefore, the HOR catalyst should have excellent affinity for H_2, which indicates that the HBE of the catalyst has a significant effect on the HOR activity [54,63-65]. A markedly high HBE is advantageous for hydrogen atom adsorption (Tafel/Heyrovsky reaction); however, a markedly low HBE is suitable for hydrogen atom desorption (Volmer reaction). Yan et al. first proposed a correlation between the HBE theory and alkaline HOR activity [66-68]. In the cyclic voltammetry (CV) curves of the Pt, Ir, Pd, and Rh catalysts, the H_{UPD} desorption peak moves toward a high potential as the electrolyte pH value increases. Assuming that HBE is linearly related to the desorption peak of H_{UPD} according to $HBE=-E_{Peak}F$, the HBE of the electrocatalyst increases as the pH value of the electrolyte increases. The HOR activity of the Pt, Ir, Pd, and Rh catalysts was

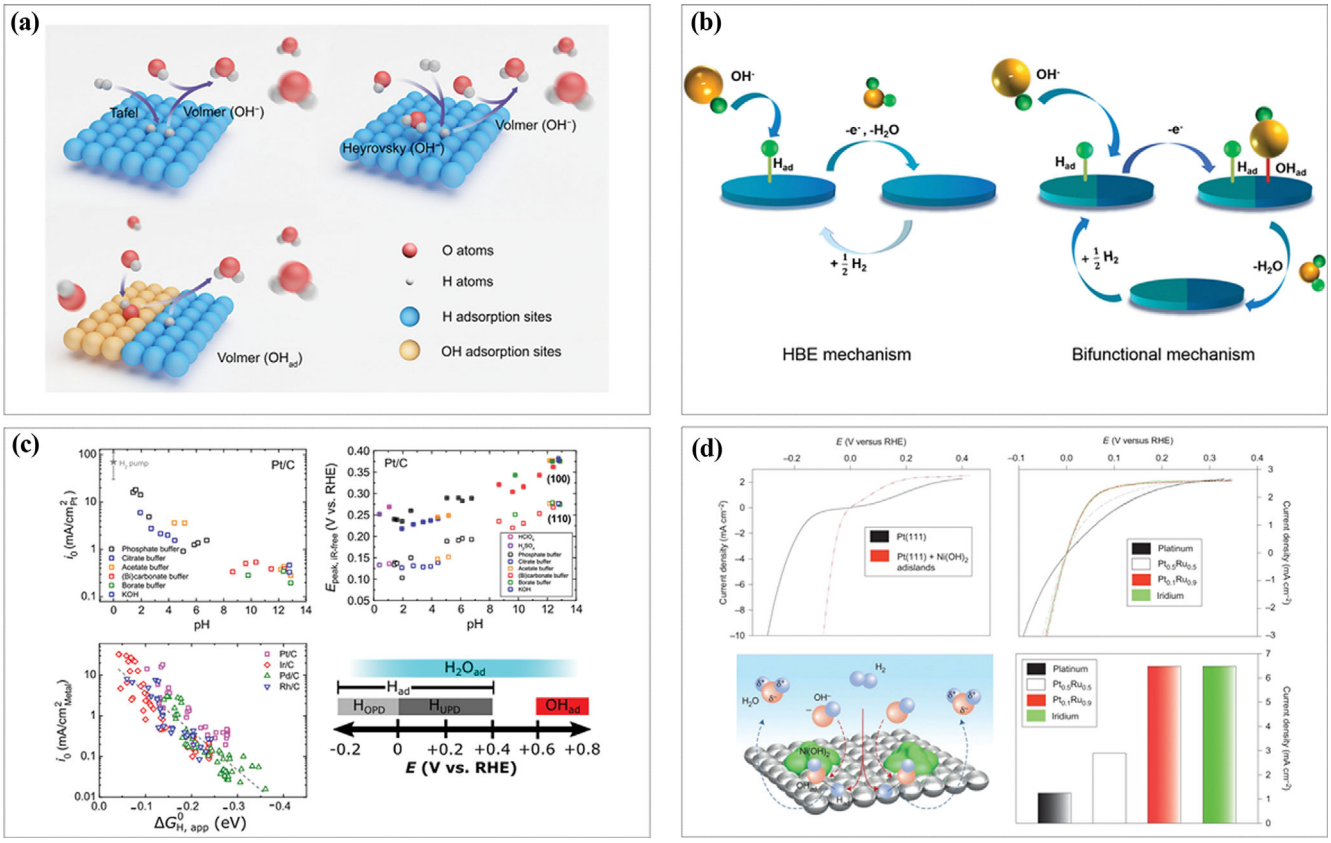

Fig. 2. (a) Schematic illustration of HOR routes in alkaline condition. Reprinted with permission from ref. 24 Copyright 2021 American Chemical Society. (b) Schematic representation of HBE mechanism and bifunctional mechanism. Reproduced with permission from ref. 53 Copyright 2020 Elsevier B. V. All rights reserved. (c) The HUPD desorption peak potential from cyclic voltammograms of Pt/C as function of pH and correlation between the exchange current density and HUPD desorption peak. Reproduced from ref. Copyright 2020 Elsevier B. V. All rights reserved. (d) The HOR activity in alkaline solution and schematic image of bifunctional catalysts ($Ni(OH)_2$/Pt(111), PtRu and Ir). Reprinted from ref. 70 Copyright 2013 Nature Publishing group.

found to decrease as the pH of the electrolyte increased (Fig. 2(c)). Zhuang et al. evaluated the HOR performance of PtNi and acid-treated PtNi nanoparticles with approximately the same HBE but different OHBEs. As expected, the PtNi catalyst supports the HBE theory by exhibiting a markedly higher HOR performance due to electron effects than the bifunctional effect [69].

In addition to the HBE theory, researchers have proposed a bifunctional effect that promotes HOR under alkaline conditions. However, the adsorbed oxygen species near H_{ad} accelerates the oxidative desorption of H_{ad}, which is the main issue of this theory. Previously, the bifunctional effects of alkaline HOR were evaluated by the Markovic group [70]. Based on their observations, the adsorption of more oxygen species in $Ni(OH)_2$ decorated Pt and PtRu alloys, resulting in improved HOR compared to that with pure Pt. Such finding demonstrates that the adsorption of OH species, called the "bifunctional effect" or "oxophilic effect," promotes alkaline HOR kinetic (Fig. 2(d)). Alia et al. also reported significantly enhanced HOR activity in monolayered Cu shells on Pt electrodes [71]. These researchers grew a Cu shell into a monolayer on Pt, as the oxygen species adsorption energy of Cu is similar to that of Ir or Ru. Accordingly, Cu acted as an OH adsorption site and the bifunctional effect was inferred to promote the kinetics of the HOR.

The mechanisms for improving HOR activity remain controversial. However, HBE and/or reactive oxygen species adsorption can be regulated by atomically adjusting the surface properties of the catalysts, which will help elucidate the actual HOR mechanism.

1. PGM-based Catalysts

The HOR activity under alkaline conditions is sensitive to structural parameters, including particle size, shape, and composition. Thus, various studies have been conducted to manipulate the structural parameters of PGM-based HOR catalysts.

Ohyama et al. reported the size-dependent HOR activity of Pt/C [72]. The commercial Pt/C was heat-treated at different temperatures to control the size of the Pt particles. The mass activity of Pt/C in 0.1 M KOH showed a maximum value at 3 nm, consistent with previous reports on the effect of Pt particle size on HOR in acidic electrolytes. Alternatively, the specific activity increased as the particle size increased, which is consistent with previous reports on the specific activity according to Pt size in acidic electrolytes. The specific activity of Pt/C converged to a certain value as particle size increased; this is because the ratio of Pt atoms on the facet to the total number of atoms on the surface increased as the particle size increased, almost reaching a plateau (Fig. 3(A)). Zheng et al. heated commercial Ir/C from 300 to 800 °C to tune the Ir parti-

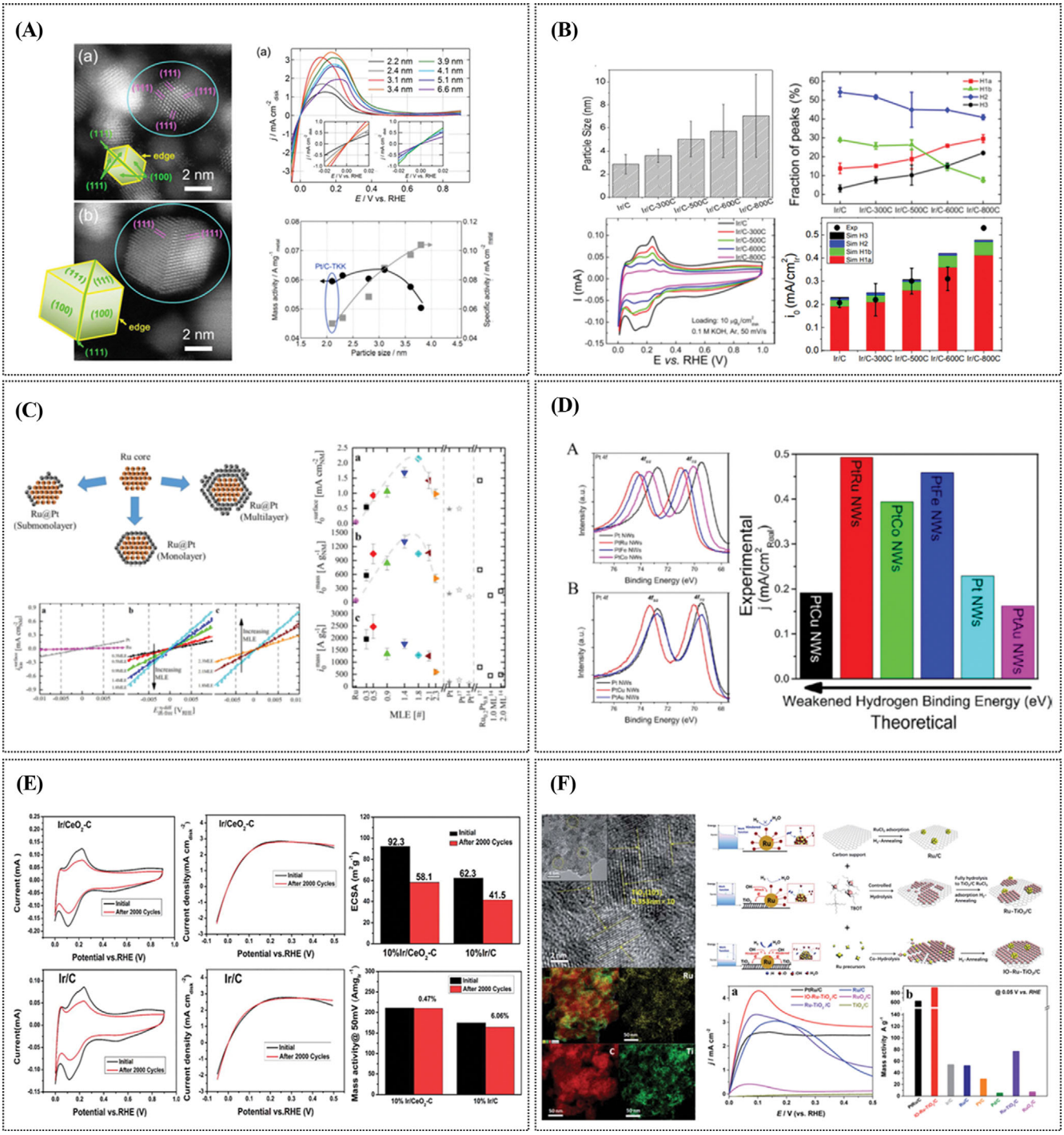

Fig. 3. (a) The effect of Ru nanoparticle size on HOR activity from alkaline electrolyte. Reprinted with permission from ref. 72 Copyright 2013 American Chemical Society. (b) Correlation between HOR activity and weak hydrogen binding site according to Ir/C catalyst particle size. Reprinted with permission from ref. 73 Copyright 2015 American Chemical Society. (c) Observation of differences in alkaline HOR activity of Ru@Pt catalyst according to Pt shell thickness. Reproduced with permission from ref. 32 Copyright 2018 Electrochemical Society (ECS). (d) Ultra-thin 1D Pt-based binary nanowires with controllable composition and their HOR activity in alkaline electrolytes. Reprinted with permission from ref. 74 Copyright 2016 American Chemical Society. (e) Variation of electrochemical properties according to the presence of CeO_2 in Ir/C. Reproduced with permission from ref. 75 Copyright 2017 Royal Society of Chemistry. (f) Preparation step, morphologies, and HOR activity of Ru-TiO_2 based catalysts. Reproduced with permission from ref. 76 Copyright 2020 Royal Society of Chemistry.

cle size from 3 to 12 nm [73]. The HOR activity of Ir/C tended to increase as the particle size increased, which indicates that as the size of the Ir particles increases, the population of low-index facets with the smallest HBE increases, and can be identified by the quanti-

fied surface site distribution through deconvolution analysis of the H_{UPD} peak (Fig. 3(B)).

Various precious metal-based alloy catalysts for HOR in alkaline electrolytes have been evaluated. Schwämmlein applied a Ru@Pt core-shell catalyst with various Pt shell thicknesses to the alkaline HOR [32]. The HOR activity of a Ru catalyst completely surrounded by Pt has been experimentally demonstrated to be superior to that of a partially covered Pt@Ru catalyst, suggesting that the HBE effect in the HOR mechanism is relatively more important than the bifunctional effect (Fig. 3(C)). Wong et al. synthesized several Pt-M alloy nanowires (M=Fe, Co, Ru, Cu, and Au) to understand the correlation between chemicals, composition, and alkaline HOR activity [74]. The HOR activity of Pt_7Ru_3 NWs in various sample groups had the highest performance relative to single Pt NWs due to the electronic interactions between Pt and the second metal. In contrast, Pt_7Cu_3 and Pt_7Au_3 exhibited relatively low HOR activity, which was determined by the formation of Cu oxide on the Pt surface and the increase in HBE, respectively (Fig. 3(D)).

To date, most HOR catalysts have been used as catalysts in which metal nanoparticles are dispersed on carbon, which has good conductivity. However, these catalysts have low stability and activity owing to the weak interactions between the metal particles and the support. Therefore, to improve the HOR activity in alkaline low electrolytes, various studies related to M-H_{ad} support that can promote the weakening of M-H_{ad} binding and facilitate the supply of OH_{ad} to metal oxides have been recently conducted.

Shao et al. synthesized Ir/C and Ir/CeO_2/C catalysts and compared their HOR activity [75]. The Ir/CeO_2/C catalyst showed 2.8- and 1.8-fold higher mass activity and specific activity than Ir/C owing to the synergy between the electronic effect and bifunctional effect. The durability test results revealed a 0.47% decrease in initial mass activity, which is significantly lower than that of Ir/C (6.06%) and is considered to be improved by strong metal support interaction (SMSI) between Ir and CeO_2 (Fig. 3(E)).

Wei et al. synthesized IO-Ru-TiO_2/C and reported an uncommon finding that Ru clusters can efficiently catalyze the HOR at a high potential range without being oxidized [76]. XAFS and XPS analyses confirmed that the Ru clusters in IO-Ru-TiO_2/C were preoxidized close to the level of Ru^{IV} and maintained a metallic surface with abundant metallic Ru-Ru bonds. This phenomenon can markedly improve HOR activity by preventing the adsorption of oxygen species during HOR. The mass activity of IO-Ru-TiO_2/C was 907 A g_{Ru}^{-1} @ 0.05 V, which was 17.5- and 1.5-fold higher than that of Ru/C and PtRu/C (Fig. 3(F)).

2. PGM-free Catalysts

To date, Raney Ni-based materials have mainly been used as HOR

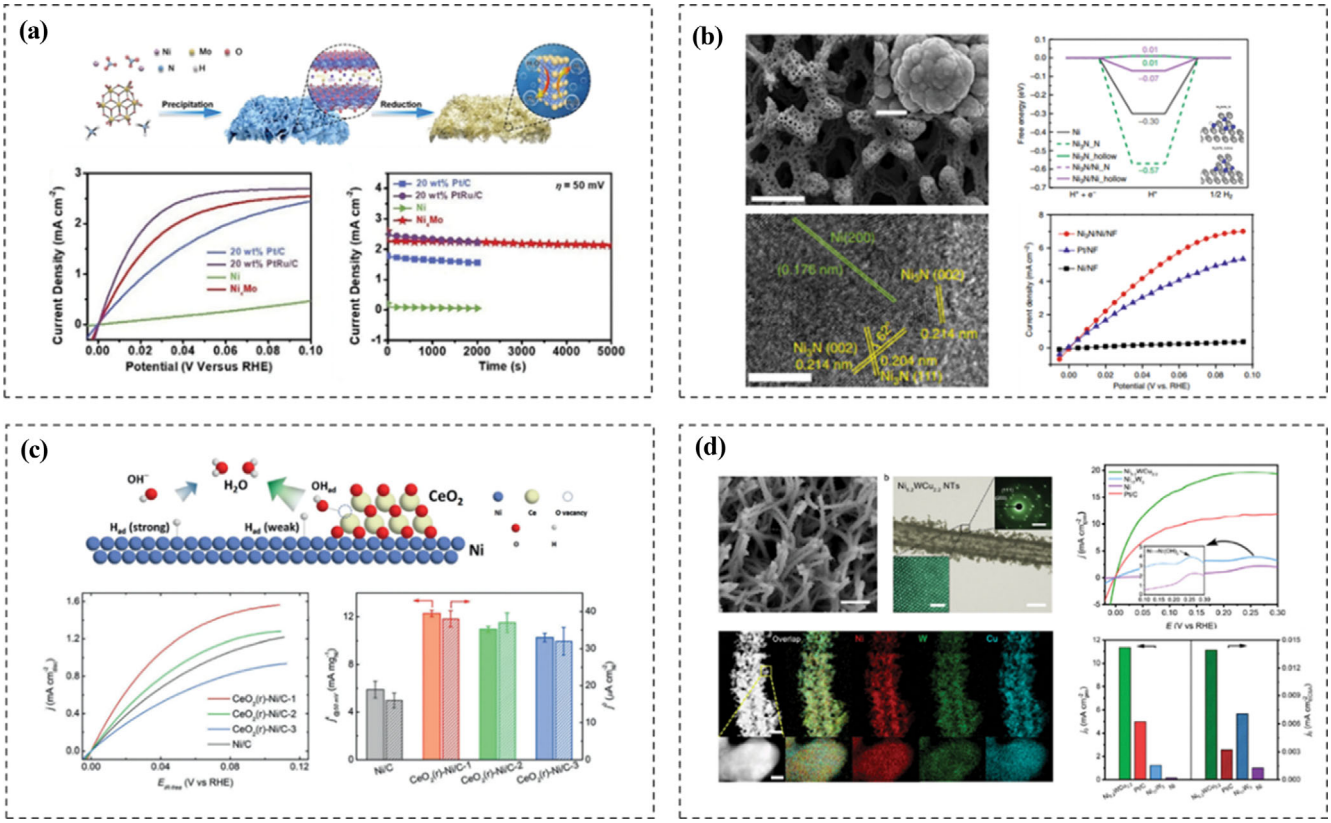

Fig. 4. (a) Schematic presentation of preparation step, HOR polarization curves, and chronoamperometric response of Ni_4Mo nanoparticles. Reproduced with permission from ref. 77. Copyright 2021 Wiley-VCH Verlag GmbH. (b) Morphologies, lattice fringes, hydrogen adsorption energy, HOR polarization curves of Ni_3N/Ni/NF. Reproduced with permission from ref. 78. (c) Schematic illustration of CeO_2-Ni during HOR process, HOR polarization curves, and HOR activity of CeO_2-Ni/C series. Reproduced with permission from ref. 79 Copyright 2019 Wiley-VCH Verlag GmbH & Co. KGaA, Weinheim. (d) Morphologies, HOR polarization curves, and HOR activity of NiWCu series. Reproduced with permission from ref. 35.

catalysts in AEMFCs; however, the replacement of PGM-based catalysts has yet to be achieved. Therefore, various efforts have been made to enhance the alkaline HOR activity of Ni-based materials.

Li et al. reported that NiMo alloys with appropriate compositions can significantly improve the HOR activity [77]. The Ni_4Mo nanocatalyst was synthesized using a two-step precautionary reduction approach. According to the DFT calculations, Ni and Mo alloys significantly weakened M-Had and improved OH adsorption. Electrochemical measurements revealed that the Ni4Mo alloy catalyst exhibited significant apparent HOR activity with J=2.2 $mAcm^{-2}$ at η=50 mV, which was close to that of PtRu/C. In addition, mass activity and exchange current density were 78.7 A g^{-1} and 26.1 A g^{-1}, respectively (Fig. 4(a)).

Sun et al. demonstrated that interfacing Ni_3N and Ni on metallic Ni foam is an effective approach for synthesizing highly active electrocatalysts for the HOR in alkaline media [78]. The DFT calculations show that the free energy change in hydrogen adsorption at the interface site of Ni_3N/Ni/NF is very close to zero, which is advantageous for hydrogen electrochemistry. The current density of Ni_3N/Ni/NF was 6.95 mA cm^{-2} at 0.09 V, which was higher than that of Pt/NF (5.25 mA cm^{-2}). The exchange current density of Ni_3N/Ni/NF was 3.08 mA cm^{-2}, which was 1.4-fold higher than that of Pt/NF. In addition, Ni_3N/Ni/NF exhibited superior durability and great resistance to CO poisoning (Fig. 4(b)).

Luo et al. reported CeO_2/Ni heterostructured catalysts designed to accelerate HOR dynamics in alkali electrolytes [79]. The synergistic electron effect between CeO_2 and Ni and the abundant oxygen vacancies of CeO_2 contribute to the CeO_2(r)Ni/C-1 hybrid catalyst with excellent HOR performance in an alkaline medium. The exchange current density and mass activity were 0.038 mA cm^{-2} and 12.28 mA mg^{-1}, which were confirmed to be excellent compared to those of previously reported non-PGM catalysts (Fig. 4(c)).

Gao et al. reported that ternary nickel-tungsten-copper alloys ($Ni_{5.2}WCu_{2.2}$ nanotubes) can enhance the HOR activity and stability in alkaline electrolytes [35]. The exchange current density and specific activity of the $Ni_{5.2}WCu_{2.2}$ nanotubes were 11.36 mA cm^{-2} and 0.014 mA cm^{-2}, respectively, which are 2.3- and 4.4-fold higher than those of commercial Pt/C, respectively. Such high HOR activity can be attributed to both the high intrinsic synergistic active sites, as revealed by the DFT and the advanced catalyst architecture for a highly exposed surface area for catalyzing the HOR. In addition, $Ni_{5.2}WCu_{2.2}$ nanotubes not only have superior HOR activity, but also

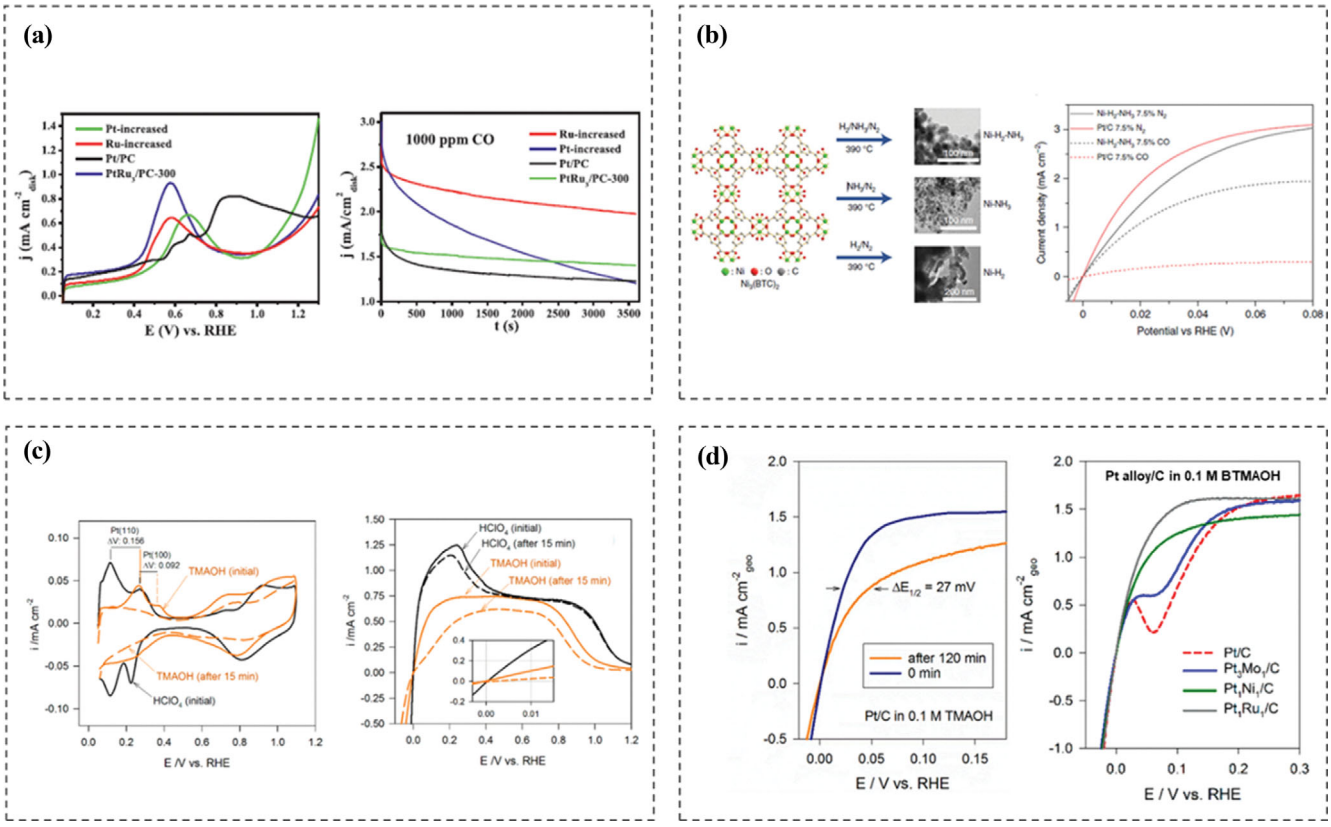

Fig. 5. (a) CO stripping voltammograms (left) and CO tolerance test (right) of PtRu based catalysts. Reproduced with permission from ref. 29 Copyright 2021 Wiley-VCH Verlag GmbH. (b) Schematic illustration and TEM images (left) and CO poisoning test compared to Pt/C (right) of Ni based metal-organic framework catalysts (Ni-H2-NH3). Reproduced with permission from ref. 40. (c) CVs (left) and HOR voltammograms (right) of Pt in 0.1 M $HClO_4$ and TMAOH electrolytes. They were obtained before and after applying 0.1 V vs RHE to Pt electrode for 15 min. Reprinted with permission from ref. 46 Copyright 2018 American Chemical Society. (d) HOR voltammograms before and after the chronoamperometry experiment at 0.1 V vs RHE for 120 min of Pt/C in 0.1 M TMAOH (left). HOR voltammograms of Pt alloy/C catalysts in 0.1 M BTMAOH (right). Reprinted with permission from ref. 47 Copyright 2017 American Chemical Society.

considerable long-term stability and anti-CO resistance (Fig. 4(d)).

3. Poisoning Issues in HOR Catalysts

CO poisoning of the catalyst surface is unavoidable unless completely pure hydrogen is not supplied. In practice, as hydrogen is supplied in its reformed form in the industrial field, a small amount of CO is introduced to the electrode. Even a very small amount of CO binds strongly to the surface of the catalyst (especially Pt), which is associated with performance degradation [39,40]. Therefore, the HOR catalyst must not only have activity but also resistance to CO. Sun et al. sought to improve the CO tolerance by utilizing the oxophilic behavior of Ru and inducing an electronic effect with Pt based on a PtRu catalyst as shown in Fig. 5(a) [29]. In particular, the Ru-increased catalysts showed a high HOR current density even in the presence of 1,000 ppm CO. On the other hand, Ni-based metal-organic framework catalysts were introduced by Yan and Hu as non-PGM catalysts (Fig. 5(b)) [38]. The proposed catalyst had a higher CO resistance than commercial Pt catalysts, suggesting that non-noble metal catalysts can also be applied in actual fuel cells.

The interaction between the ionomer and catalyst is another critical issue in AEMFC, and actually anion exchange ionomers (AEI) are known to influence HOR activity. Cation-hydroxide-water can be co-adsorbed on catalyst surfaces, such as Pt, which adversely affects the HOR activity as shown in Fig. 5(c) [44]. Co-adsorption blocks the active sites of the catalyst and generates barriers that prohibit the access to hydrogen [45]. Kim et al. observed that tetramethylammonium hydroxide (TMAOH), which contains the main polymers used in AEM, can decrease the HOR activity of Pt catalysts [47]. As illustrated in Fig. 5(d), the Pt/C catalyst in TMAOH organic solution had a significantly lower HOR current density after chronoamperometry at 0.1 V vs. reversible hydrogen electrode (RHE). The Pd based electrocatalysts show the potential alternatives for Pt based electrocatalysts due to the less adsorption energy to the AEIs. However, low HOR activity compared to Pt and high affinity to phenyl groups hinder its proper choice as an alkaline HOR electrocatalysts. The phenyl groups in benzyltrimethylammonium hydroxide (BTMAOH) organic solution had a more severe effect than TMAOH owing to its phenyl groups adsorption Fig. 5(d) [47]. The Ru species in the Pt-Ru/C catalyst can prevent the adsorption of phenyl groups. These adsorption issues must be considered to obtain the complete performance of AEMFC, and to solve this problem, it is necessary to change the adsorption energy through catalyst surface modifications.

ORR IN ALKALINE ENVIRONMENTS

The oxygen reduction reaction (ORR) is crucial in AEMFC. Compared to HOR, ORR is a sluggish reaction that consists of multiple adsorption/desorption and reaction steps involving oxygen-containing species, such as O, OH, O_2^-, HO_2^-, and H_2O_2 [80,81]. This complex reaction step in an alkaline environment can be written as:

$$O_2+2H_2O+4e^- \leftrightarrow OOH^*+H_2O+OH^-+3e^-$$
$$OOH^*+H_2O+OH^-+3e^- \leftrightarrow O^*+H_2O+2OH^-+2e^-$$
$$O^*+H_2O+2OH^-+2e^- \leftrightarrow OH^*+3OH^-+e^-$$
$$OH^*+3OH^-+e^- \leftrightarrow 4OH^-$$

The ORR proceeds via different pathways in alkaline media relative to acidic media. The Markovic group reported a modified form of the Pourbaix diagram of the ORR [82]. The initial electron transfer step is pH-independent, and the reversible potential for the ORR should be independent. However, if the electrode potential is revised by the reversible hydrogen electrode (RHE) scale (considering the pH dependence of the overall process), the overpotential for the ORR will be pH-dependent, and the polarization curves will shift according to the pH difference. As shown in Fig. 6(a), the overpotential of ORR at pH=1 is markedly higher than that at pH=14 and the 2-electron ORR overpotential is lower at pH=14, which is a highly alkaline medium. This pH-dependent behavior implies that ORR kinetics is markedly faster in alkaline media than acidic media.

The double-layer structure during the ORR under acidic and alkaline conditions is quite different [83] (Fig. 6(b)). In acidic media, the primary constituents are hydronium ions (H_3O^+), supporting anions, solvated molecular oxygen, and water molecules. Under these conditions in an acidic medium, chemisorbed molecular O_2, hydroxyl species (OH^-), and solvent water dipoles form the inner Helmholtz plane (IHP). Solvated molecular O_2 and anions fill the outer Helmholtz plane (OHP). Therefore, the ORR proceeds by only chemisorbed molecular O_2 until $4e^-$ and $4H^+$ are transferred, followed by desorption of stable H_2O molecules as the final product. However, in alkaline media, although the double-layer structure is not significantly different, some important aspects must be considered. When the pH is high, the water molecules not only act as a solvent, but also as a source of protons. In the IHP, the OH^- molecules, solvent water dipoles, and chemisorbed O_2 are adsorbed. In this system, the surface contains more OH^-, and the solvated oxygen species can be stabilized in the outer Helmholtz plane, resulting in competition between the outer and inner sphere electron transport mechanisms, indicating that the ORR can proceed by either inner-sphere or outer-sphere electron transfer.

Due to kinetic advantages in the alkaline electrolyte, catalyst options may vary widely. Fig. 6(c) shows the polarization curves of three typical ORR catalysts, which show the changes in behavior in acid and alkaline electrolytes [84]. First, Pt/C, a typical platinum catalyst, shows almost similar ORR activity despite its kinetic advantages in the alkaline electrolyte, which is due to OH^- species adsorbed on the platinum surface in the alkaline electrolyte. In the alkaline electrolyte of OH^- having a higher concentration than the acid electrolyte, the density of the active site of platinum is reduced due to the adsorption of OH^- in the surface of platinum, thereby exhibiting relatively low ORR activity. This can be seen from the comparison of Ring current, it can be seen that H_2O_2, which is a result of 2 electron ORR reaction, is hardly generated in the acid electrolyte, whereas a relatively large amount of H_2O_2 is generated in the alkaline electrolyte. On the other hand, it may be seen that Ru/C and FeTPP/C having a relatively low ORR activity compared to platinum show higher activity in the alkaline electrolyte, which is due to the kinetic advantages in the alkaline electrolyte and the ORR reaction through outer-sphere electron transfer. Therefore, in the alkaline electrolyte, it is possible to use various catalysts other than platinum, and through this, many studies have been conducted to develop catalysts that can replace platinum. Therefore, PGM based ORR electrocatalysts have less attention due to the various cata-

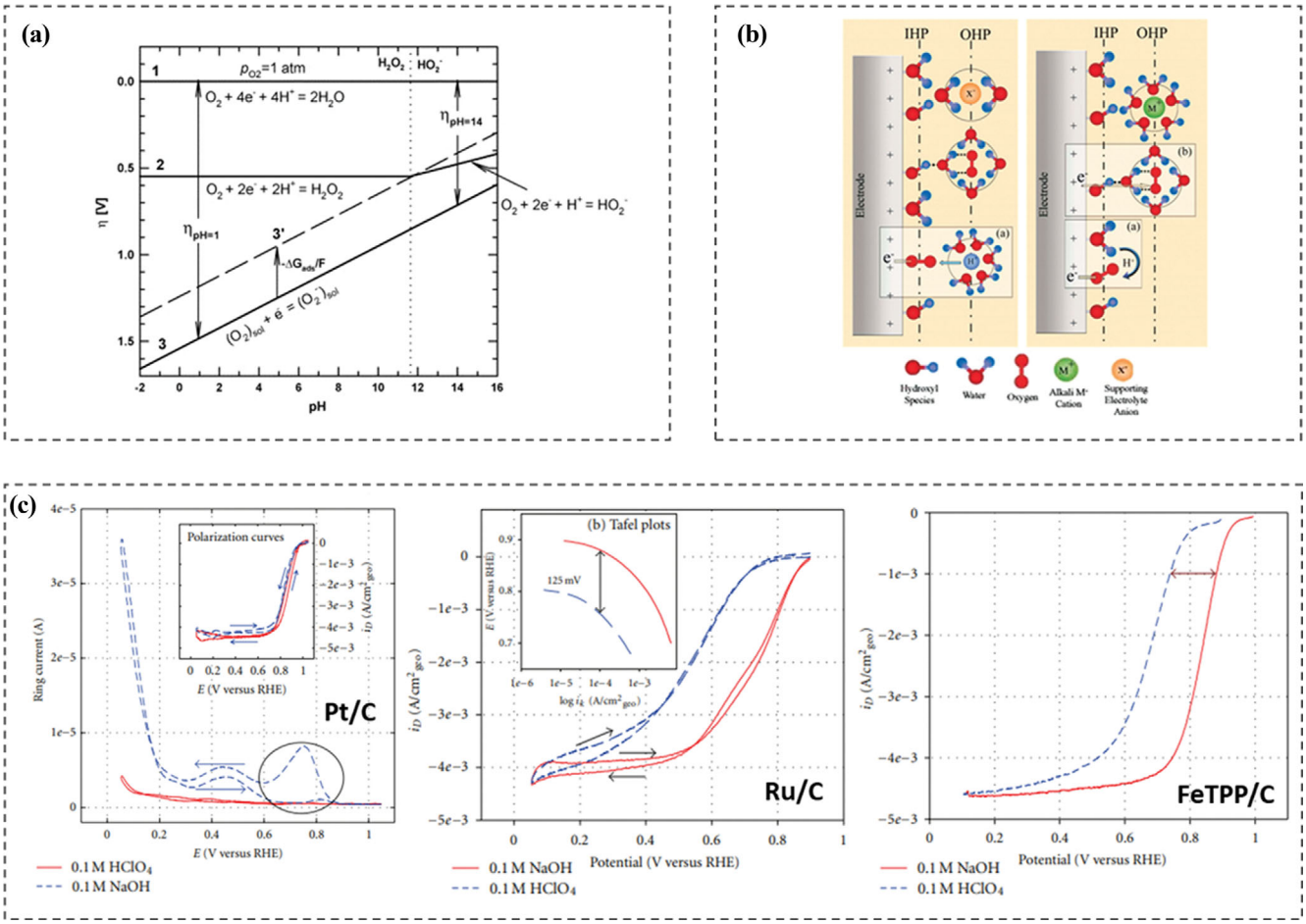

Fig. 6. (a) Modified form of the Pourbaix diagram of the ORR. Reproduced with permission from ref. 82. Copyright 2007 Elsevier. (b) Schematic presentation of double-layer structure during the ORR under acidic and alkaline conditions. Reprinted with permission from ref. 83. Copyright 2011 American Chemical Society. (c) The ORR polarization curves of three representative catalyst for ORR. Reproduced with permission from ref. 84. Copyright 2011 Hindawi Publishing Corporation.

lysts choices in alkaline ORR. Several studies are still being conducted to reduce PGM loadings such as low-content Pt catalysts with core-shell or alloy structures; PtNi, PtCo, PtFe etc. However, due to its high cost and scarcity of platinum, great alternatives such as Non-PGM based ORR catalysts have excellent attention to replace the platinum-based electrocatalysts in AEMFCs.

1. Transition Metal-based Catalysts

Traditionally, Pt-based catalysts have been used as reference materials in AEMFC. However, several problems regarding Pt catalysts and the development of non-precious-metal-based catalysts have led to the expansion of catalyst selection for AEMFC. Among the various non-precious metal-based catalysts, transition metal-based catalysts can be applied as ORR catalysts [21,85,86]. The ORR mechanism of transition metal-based catalysts involves the interaction of O_2 with metallic oxide catalysts, which can be explained by the inorganic chemistry principles of molecular orbitals and crystal field theory. Several transition metal oxide catalysts have been intensively evaluated and among them, spinel oxides have attracted considerable attention owing to their good activity and stability. The spinel, in the general formulation of AB_2O_4, has oxide anions arranged in a cubic close-packed lattice, where 1/8th of the tetrahedral sites are occupied by A atoms, and half of the octahedral sites are occupied by B atoms. The ORR activity of spinel oxides can be tuned by changing the composition of the A and B atoms.

Zhuang et al. reported Mn-Co spinel oxide catalysts with high activity and stability. These researchers first applied a Mn-Co spinel catalyst to an AEMFC and outperformed the conventional Pt-based AEMFC [87]. The power density of the cell employing the Mn-Co cathode reached 1.1 W cm^{-2} at 2.5 A cm^{-2} at 60 °C. Their in-depth characterization showed that the remarkable performance is due to the synergistic effect of Mn sites binding O_2 and Co sites, activating H_2O to promote the proton-coupled electron transport process. This electrocatalytic synergistic effect is pivotal for high-rate oxygen reduction, especially under water depletion/low-humidity conditions.

Hyeon et al. reported (001) facet-enclosed and strain-free Co-Mn spinel oxide surfaces, which were synthesized via template-based epitaxial growth on Co_3O_4 nanocubes [88]. These researchers changed the ratio of Co to Mn and explored the effects of Co and Mn composition. In this system, the ORR activity showed a volcano-like trend with Mn/Co ratios due to adequate charge transfer from the octahedral Mn to neighboring Co. Among various

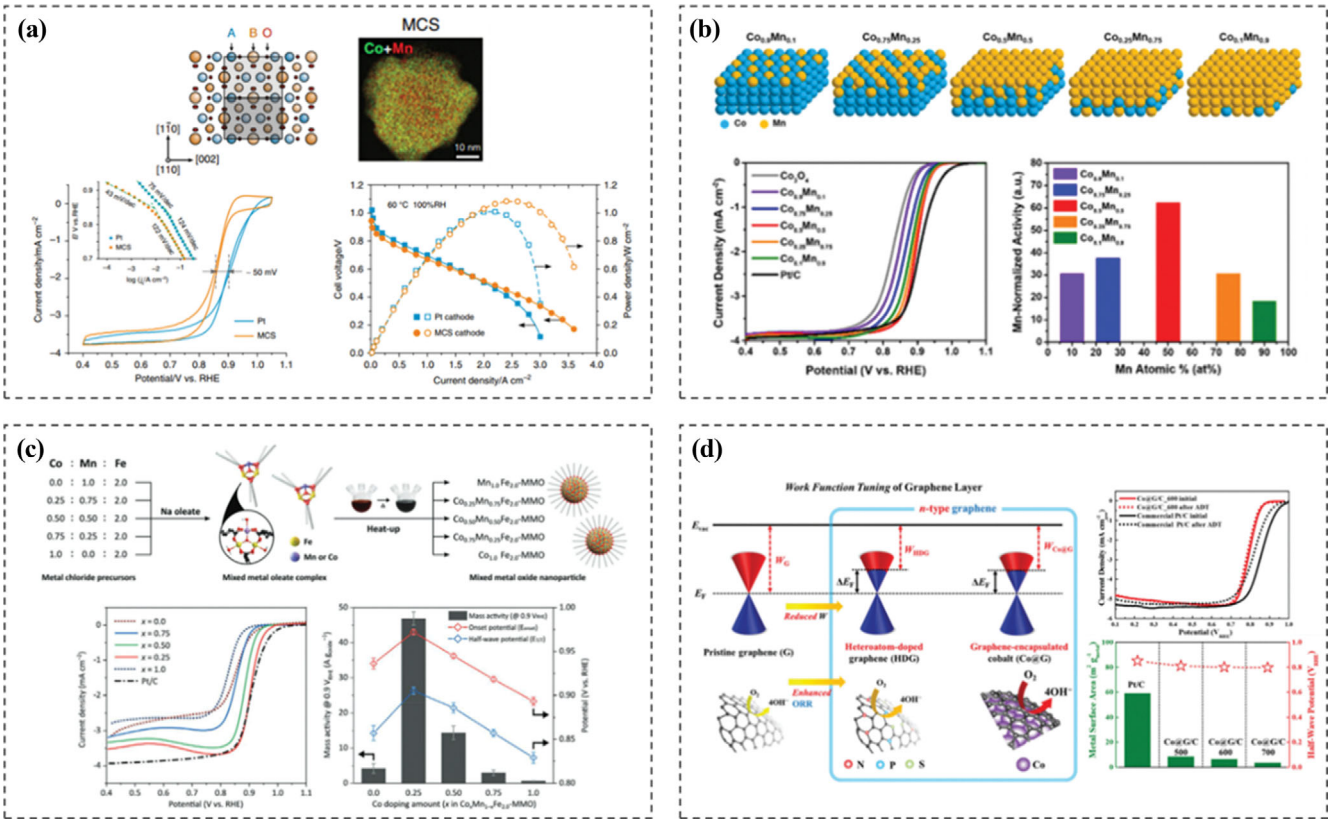

Fig. 7. (a) Schematic presentation of structure, TEM EDX mapping, ORR polarization curves and AEMFC performance of Mn-Co spinel oxide. Reproduced with permission from ref. 87. Copyright 2019 Springer Nature. (b) Schematic illustration of preparation of Mn-Co samples, ORR polarization curves and performances. Reprinted with permission from ref. 88. Copyright 2022 American Chemical Society. (c) Schematic illustration of preparation of Co-Mn-Fe oxide, ORR polarization curves and it performances Reproduced with permission from ref. 89. Copyright 2022 Wiley-VCH Verlag GmbH. (d) Schematic presentation of structure of Co@C/C catalyst, ORR polarization curves and its activity. Reproduced with permission from ref. 90. Copyright 2019 Royal Society of Chemistry.

compositions, the $Co_{0.5}Mn_{0.5}$, which is the optimized ratio, showed high ORR activity (0.894 V vs. RHE in 1 M KOH) and stability (2% activity loss against chronoamperometry). By controlling the facets and strain, a well-defined platform was established for investigating the composition-structure-activity relationships in electrocatalytic processes.

Sung et al. synthesized well-controlled Mn-, Fe-, and Co-based ternary oxide model catalysts using the heat-up method, and explored the contribution of each transition metal species to the measured ORR activity [89]. As shown in Fig. 7(b), Co was incorporated into manganese ferrite. This incorporated Co increased the Mn oxidation state and moved Fe from the O_h site to the T_d site, indicating that Mn is preferentially occupied at the O_h site. The addition of an optimal amount of Co optimized the electronic structure of Mn, resulting in high intrinsic ORR activity. As a result, the rationally designed $Co_{0.25}Mn_{0.75}Fe_{2.0}$-oxide nano-catalyst exhibited a high half-wave potential of 0.904 V (relative to RHE) and a mass activity of 46.9 A g oxide-1 in addition to promising electrocatalytic stability. Ultimately, these researchers provided a potentially new avenue for the design and understanding of the catalytically active origins of spinel oxides with respect to their structural and constitutive properties.

Yoo et al. revealed a new class of catalysts, which is a work function tailored to graphene via the adoption of 3D graphene shell encapsulated cobalt nanoparticles (Co@G/C_600) to efficiently activate the graphene shell as an ORR active site [90]. In this assessment, the cobalt core functions as a fully sealed donor, facilitating graphitization and charge transfer to the outer graphene shell, resulting in n-type nanographene. Owing to their favorable 3D structure, these n-type graphene catalysts induced high utilization of active sites in the outer graphene shell. Additionally, the outer graphene shell acted as a protective layer against the dissolution/agglomeration of metal nanoparticles. As a result, this catalyst had ORR catalytic activity comparable to that of the commercial Pt/C catalyst with higher durability than the commercial Pt/C catalyst in alkaline media. The MEA using the 40 wt% Co@G/C_600 catalyst at the cathode had a high power density of 412 mW cm^{-2}, which is one of the best values for non-precious metal-based AEMFC reported to date. Consequently, tailoring the work function through graphene shell encapsulation of transition metals serves as a powerful approach for the fabrication of highly durable non-precious metal nanostructures and provides new insights into advanced AEMFC cathode catalyst design.

2. Carbon-based Catalysts

Carbon materials doped with transition metals and nitrogen (M-N-C, M=Fe, Co, and Mn) have received remarkable attention owing to their high activity and relatively high stability [91-93]. In

particular, among them, as the Fe-based Fe-N-C catalyst displayed the highest activity, it is expected to be a material that can replace the platinum catalyst in AEMFC. As the active site of the Fe-N-C catalyst is considered to be an Fe-N_x structure in which Fe is bonded with nitrogen, increasing the density of the active site is a very important issue to increase the ORR activity [94,95]. In general, the best-known synthesis method for M-N-C catalysts is the simultaneous high-temperature heat treatment of a nitrogen-containing material, a metal precursor, and a carbon support. Catalysts produced through heat treatment exhibit high ORR activity [96]. However, for catalysts made by mixing simple precursor materials and heat treatment, controlling the catalyst active sites is difficult. In addition, it is difficult to control the pyrolysis processes used to create useful random porous structures for catalyst supports to achieve the desired pore size and surface composition.

To investigate the influence of the porous structure on the catalyst function, Hyeon et al. designed three types of N-doped carbon model catalysts with different ratios of micro-, meso-, and macropores, as shown in Fig. 8(a) [97]. The pore structure was precisely controlled, and model catalysts were prepared to demonstrate the effect of the porous structure of the carbon-based catalysts. Based on physicochemical characterization and electrochemical analysis, the researchers concluded that the pore size of the carbon catalyst, which contributes to the electrolyte wetting of the surface area, is in the mesopore range, whereas macropores promote the kinetic accessibility of the active sites. Based on their findings, these researchers prepared an optimized Fe-N-C catalyst that exhibited the best ORR performance in alkaline media with excellent long-term stability in anion exchange membrane fuel cells. Overall, their work established the basis for the theoretical design of porous carbon structures for electrocatalytic applications.

The porous structure of carbon-based materials is crucial for achieving a high ORR activity in alkaline media [98,99]. Therefore, the design of porous structures is one of the main issues in carbon-based ORR catalysts. A representative method to design porous carbon involves the use of a sacrificial template to generate a porous structure. Yoo et al. reported unprecedented single-atom ORR activity of Fe, Si, and N co-doped carbon (FeSiNC) supported on 3D interconnected mesoporous carbons (25 and 50 nm) derived from silica hard templates [100]. The Si moiety connected to the carbon surface was involved in the formation of atomically distributed $FeSi_xN_{4-x}$ sites through Si substitution at the N position of the Fe-N_4 site, which is the ORR active site of Fe-N-C. Fe-Si-N-C with larger mesopores (50 nm) exhibited improved single-cell performance owing to superior ORR activity and improved mass transport properties. Lee et al. synthesized ordered mesoporous Fe-N-C

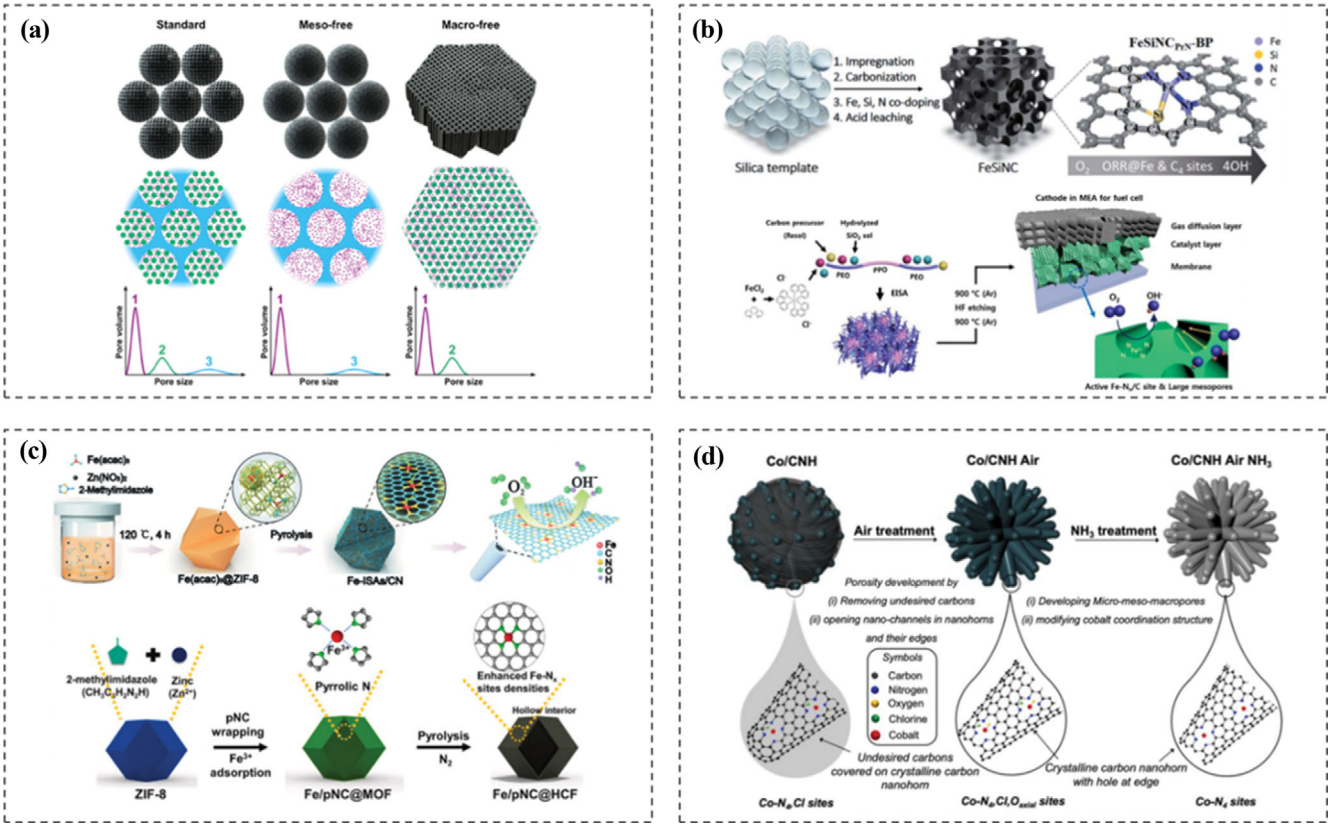

Fig. 8. (a) Schematic illustration of porous structure of carbon based catalysts. Reprinted with permission from ref. 97. Copyright 2019 American Chemical Society. (b) Schematic presentation of template based synthesis of carbon based catalysts. Reproduced with permission from ref. 100. Copyright 2019 Royal Society of Chemistry. Reproduced with permission from ref. 14. Copyright 2018 Elsevier (c) Schematic illustration of synthesis of ZIF-8 based porous carbon catalysts Reproduced with permission from ref. 103. Copyright 2022 Wiley-VCH Verlag GmbH. Reproduced with permission from ref. 104. Copyright 2021 Elsevier (d) Schematic presentation of synthetic procedure of porous nano-horn carbon. Reproduced with permission from ref. 105. Copyright 2022 Elsevier.

with highly active Fe-N_x/C sites, denoted as m-FePhen-C, as a cathode catalyst for the oxygen reduction reaction in AEMFC [14]. Using a simple block co-polymer-assisted soft-template method, these researchers directly prepared mesoporous Fe-N-C with high catalytic performance and demonstrated that the generation of the Fe-N_x/C active sites and the formation of an ordered mesoporous structure were achieved simultaneously in a simple soft-template-assisted process.

Recently, the use of metal organic frameworks (MOFs) as templates for heat-treatment precursors has been actively reported. Among various MOFs, the zeolitic imidazolate framework (ZIF) is one of the most suitable MOFs, and a nitrogen-doped porous carbon catalyst with a high surface area can be synthesized by simple carbonization owing to the sublimation characteristic of zinc [101, 102]. In the process of synthesizing ZIF, the M-N-C catalyst can be easily synthesized by simply adding a metal precursor. Li et al. reported a highly reactive and stable isolated single-atom Fe-N-doped porous carbon (ISA Fe/CN) catalyst with an Fe loading of up to 2.16 wt% [103]. This catalyst displayed excellent ORR performance with a half-wave potential ($E_{1/2}$) of 0.900 V, outperforming commercial Pt/C. Owing to the cage-encapsulated-precursor pyrolysis strategy, they showed a high loading of single-atomic Fe-N_x sites with high ORR activity. As the M-N-C catalyst may be easily prepared with only the addition of such a simple metal, many research groups have revealed various M-N-C catalysts using a combination of ZIF and transition metals. Yoo et al. devised a strategy to increase the number of Fe-N_x sites using the electrostatic interaction between electronegative pyrrolic-N and electronegative Fe ions [104]. This pyrrolic N wrapping strategy can maximize the number of single-atomic Fe-N_x sites that show a high current density of 437 mA cm^{-2} at 0.6 V and a power density of 343 mW cm^{-2} in AEMFC.

A hierarchical pore structure is crucial for effective mass transfer and the utilization of a number of active sites in single-metal atom-embedded porous carbon catalysts. Yoo et al. presented a new strategy for developing a hierarchical porous structure in single-wall carbon nanohorns with Co-N_x sites (Co/CNH) and maximizing their oxygen reduction activity [105]. The optimized combination of air and ammonia annealing led to the successful construction of a hierarchical pore structure by removing amorphous carbon and opening both the inter- and intra-nanohorn channels. The Co/CNH Air NH3 catalyst had a highly superior ORR kinetic density of 60.16 mAcm^{-2} at 0.8 V in half-cell experiments, 7.3-fold higher than that of commercial Pt/C. DFT calculations revealed that the enhanced intrinsic ORR catalytic activity was due to the axial coordination of water molecules to Co-N_4, which resulted in increased overall oxophilicity and ORR activity. The AEMFC test showed a maximum power density of 742 mWcm^{-2}, which is a remarkably high performance of the M-N-C catalysts based on AEMFC. This approach can be applied to generate hierarchical porosity in bottom-up synthesized SACs and provide guidance for the design of efficient M-N-C electrocatalysts for AEMFCs.

CONCLUSIONS AND PERSPECTIVE

In summary, electrocatalysts play a pivotal role in determining the performance and cost of AEMFCs. As a large proportion of catalysts is used in commercialization, research on catalysts for the HOR and ORR in AEMFCs has been ongoing for decades. Fundamental studies on the factors that determine activity based on the mechanism have been extensively conducted. As HOR is a process in which hydrogen is adsorbed and desorbed by the catalyst surface, the intrinsic H adsorption energy of the catalyst can be a dominant descriptor in determining the HOR activity, which is explained by the HBE theory. Another theory for determining the HOR activity is the bifunctional mechanism. In the first mechanism, oxophilic materials participate in hydroxyl adsorption and affect the HOR activity. The debate on the actual determinants based on this mechanism contributes to the development of better HOR catalysts. Although electrode materials rely on PGM, related research has been carried out to reduce the amount of noble metals through structural optimization by controlling the size, morphology, and composition of the catalysts. The performance of Ni-based PGM-free catalysts is insufficient compared to that of PGM, and catalysts with improved performance have been continuously reported. In addition to HOR activity, CO poisoning and bulky cation adsorption accompanied by the use of AEI are still considered challenges to be overcome. Thus, catalysts that can achieve both high activity and durability while reducing costs are essential. However, the issue associated with ORR is the replacement of conventional Pt catalysts with non-precious metal or metal-free catalysts based on earth-abundant materials. The advantageous ORR pathway at higher pH has enabled the use of metal oxide or carbon-based catalysts, which have shown comparable performance to conventional Pt catalysts at the half-cell level. For transition metal oxide-based catalysts, the interaction between the orbitals of the metal oxide and adsorbed oxygen is considered to be a determinant of the intrinsic ORR activity in addition to the conductivity of the metal oxide. The case with carbon-based catalysts (M-N-C) is mainly determined by the dopant/co-dopant, porosity, and conductivity. Despite remarkable efforts to develop non-precious-material-based catalysts, replacing PEMFC with AEMFC remains difficult. For AEMFC, a relative latecomer, to replace PEMFC, securing price competitiveness should be the top priority. At the half-cell level, it exhibits activity comparable to that of conventional Pt/C, while at the single-cell level, it exhibits lower performance. This is because compared to Pt/C, when non-precious-material-based catalysts were applied to MEA, the electrode thickness increased, which was related to the mass transport resistance. Consequently, the development of catalysts for AEMFCs should be accompanied by improvements in electrode structures. As electrodes account for a significant portion of the cost of a fuel cell stack, developing an efficient catalyst can markedly contribute to accelerating the commercialization of AEMFCs. AEMFCs with price merits will be a leading energy conversion device for upcoming eco-friendly generation with PEMFCs.

ACKNOWLEDGEMENTS

This work was supported by the National Research Foundation of Korea (NRF) grant funded by the Korea government (2021M3H4A1A02042948, 2021M3H4A3A02086681). This work was also

supported by the New & Renewable Energy Core Technology Program of KETEP (20203020030010) in Korea.

REFERENCES

1. A. M. Oliveira, R. R. Beswick and Y. Yan, *Curr. Opin. Chem. Eng.*, **33** (2021).
2. M. Yue, H. Lambert, E. Pahon, R. Roche, S. Jemei and D. Hissel, *Renew. Sust. Energy Rev.*, **146** (2021).
3. F. Xiao, Y. C. Wang, Z. P. Wu, G. Chen, F. Yang, S. Zhu, K. Siddharth, Z. Kong, A. Lu, J. C. Li, C. J. Zhong, Z. Y. Zhou and M. Shao, *Adv. Mater.*, **33**, e2006292 (2021).
4. R. L. Borup, A. Kusoglu, K. C. Neyerlin, R. Mukundan, R. K. Ahluwalia, D. A. Cullen, K. L. More, A. Z. Weber and D. J. Myers, *Curr. Opin. Electrochem.*, **21**, 192 (2020).
5. A. G. Olabi, T. Wilberforce and M. A. Abdelkareem, *Energy*, **214** *(*2021).
6. Y. Wang, D. F. Ruiz Diaz, K. S. Chen, Z. Wang and X. C. Adroher, *Mater. Today*, **32**, 178 (2020).
7. Y. Wang, Y. Pang, H. Xu, A. Martinez and K. S. Chen, *Energy Environ. Sci.*, **15**, 2288 (2022).
8. Y. Luo, Y. Wu, B. Li, T. Mo, Y. Li, S.-P. Feng, J. Qu and P. K. Chu, *J. Energy Storage*, **42** (2021).
9. M. Liu, Z. Zhao, X. Duan and Y. Huang, *Adv. Mater.*, **31**, e1802234 (2019).
10. J. K. Norskov, J. Rossmeisl, A. Logadottir, L. Lindqvist, J. R. Kitchin, T. Bligaard and H. Jonsson, *J. Phys. Chem. B*, **108**, 17886 (2004).
11. X. Zhu, X. Tan, K. H. Wu, S. C. Haw, C. W. Pao, B. J. Su, J. Jiang, S. C. Smith, J. M. Chen, R. Amal and X. Lu, *Angew. Chem. Int. Ed. Eng.*, **60**, 21911 (2021).
12. X. Ren, B. Liu, X. Liang, Y. Wang, Q. Lv and A. Liu, *J. Electrochem. Soc.*, **168** (2021).
13. C. He, J. J. Zhang and P. K. Shen, *J. Mater. Chem. A*, **2** (2014).
14. Y. Mun, M. J. Kim, S.-A. Park, E. Lee, Y. Ye, S. Lee, Y.-T. Kim, S. Kim, O.-H. Kim, Y.-H. Cho, Y.-E. Sung and J. Lee, *Appl. Catal. B: Environ.*, **222**, 191 (2018).
15. J. A. Varnell, J. S. Sotiropoulos, T. M. Brown, K. Subedi, R. T. Haasch, C. E. Schulz and A. A. Gewirth, *ACS Energy Lett.*, **3**, 823 (2018).
16. J. Y. Choi, L. J. Yang, T. Kishimoto, X. G. Fu, S. Y. Ye, Z. W. Chen and D. Banham, *Energy Environ. Sci.*, **10**, 296 (2017).
17. K. Kumar, P. Gairola, M. Lions, N. Ranjbar-Sahraie, M. Mermoux, L. Dubau, A. Zitolo, F. Jaouen and F. Maillard, *ACS Catal.*, **8**, 11264 (2018).
18. B. G. Pollet, S. S. Kocha and I. Staffell, *Curr. Opin. Electrochem.*, **16**, 90 (2019).
19. S. Du, *Engineering*, **7**, 33 (2021).
20. A. Sajid, E. Pervaiz, H. Ali, T. Noor and M. M. Baig, *Int. J. Energy Res.*, **46**, 6953 (2022).
21. Y. Wang, J. Li and Z. Wei, *J. Mater. Chem. A*, **6**, 8194 (2018).
22. T. B. Ferriday and P. H. Middleton, *Int. J. Hydrogen Energy*, **46**, 18489 (2021).
23. L. Yang, J. Shui, L. Du, Y. Shao, J. Liu, L. Dai and Z. Hu, *Adv. Mater.*, **31**, e1804799 (2019).
24. Z. C. Yao, T. Tang, Z. Jiang, L. Wang, J. S. Hu and L. J. Wan, *ACS Nano*, **16**, 5153 (2022).
25. J. Hu, K. A. Kuttiyiel, K. Sasaki, C. Zhang and R. R. Adzic, *J. Electrochem. Soc.*, **165**, J3355 (2018).
26. W. Sheng, H. A. Gasteiger and Y. Shao-Horn, *J. Electrochem. Soc.*, **157** (2010).
27. J. Durst, A. Siebel, C. Simon, F. Hasché, J. Herranz and H. A. Gasteiger, *Energy Environ. Sci.*, **7**, 2255 (2014).
28. T. Zhao, G. Wang, M. Gong, D. Xiao, Y. Chen, T. Shen, Y. Lu, J. Zhang, H. Xin, Q. Li and D. Wang, *ACS Catal.*, **10**, 15207 (2020).
29. J. Zhang, X. Qu, L. Shen, G. Li, T. Zhang, J. Zheng, L. Ji, W. Yan, Y. Han, X. Cheng, Y. Jiang and S. Sun, *Small*, **17**, e2006698 (2021).
30. C. Zhan, Y. Xu, L. Bu, H. Zhu, Y. Feng, T. Yang, Y. Zhang, Z. Yang, B. Huang, Q. Shao and X. Huang, *Nat. Commun.*, **12**, 6261 (2021).
31. D. J. Weber, C. Dosche and M. Oezaslan, *J. Mater. Chem. A*, **9**, 15415 (2021).
32. J. N. Schwämmlein, B. M. Stühmeier, K. Wagenbauer, H. Dietz, V. Tileli, H. A. Gasteiger and H. A. El-Sayed, *J. Electrochem. Soc.*, **165**, H229 (2018).
33. W. Ni, A. Krammer, C. S. Hsu, H. M. Chen, A. Schuler and X. Hu, *Angew. Chem. Int. Ed. Eng.*, **58**, 7445 (2019).
34. Y. Gao, H. Peng, Y. Wang, G. Wang, L. Xiao, J. Lu and L. Zhuang, *ACS Appl. Mater. Interfaces*, **12**, 31575 (2020).
35. S. Qin, Y. Duan, X. L. Zhang, L. R. Zheng, F. Y. Gao, P. P. Yang, Z. Z. Niu, R. Liu, Y. Yang, X. S. Zheng, J. F. Zhu and M. R. Gao, *Nat. Commun.*, **12**, 2686 (2021).
36. F. Yang, P. Han, N. Yao, G. Cheng, S. Chen and W. Luo, *Chem. Sci.*, **11**, 12118 (2020).
37. J.-T. Ren, Y.-S. Wang, Y.-J. Song, L. Chen and Z.-Y. Yuan, *Appl. Catal. B: Environ.*, **309** (2022).
38. W. Ni, T. Wang, F. Heroguel, A. Krammer, S. Lee, L. Yao, A. Schuler, J. S. Luterbacher, Y. Yan and X. Hu, *Nat. Mater.*, **21**, 804 (2022).
39. V. F. Valdés-López, T. Mason, P. R. Shearing and D. J. L. Brett, *Prog. Energy Combust. Sci.*, **79** (2020).
40. Y. Duan, Z. Y. Yu, L. Yang, L. R. Zheng, C. T. Zhang, X. T. Yang, F. Y. Gao, X. L. Zhang, X. Yu, R. Liu, H. H. Ding, C. Gu, X. S. Zheng, L. Shi, J. Jiang, J. F. Zhu, M. R. Gao and S. H. Yu, *Nat. Commun.*, **11**, 4789 (2020).
41. B. Shabani, M. Hafttananian, S. Khamani, A. Ramiar and A. A. Ranjbar, *J. Power Sources*, **427**, 21 (2019).
42. M. Ma, G. Li, W. Yan, Z. Wu, Z. Zheng, X. Zhang, Q. Wang, G. Du, D. Liu, Z. Xie, Q. Kuang and L. Zheng, *Adv. Energy Mater.*, **12** (2022).
43. G. A. Camara, E. A. Ticianelli, S. Mukerjee, S. J. Lee and J. McBreen, *J. Electrochem. Soc.*, **149** (2002).
44. H. T. Chung, U. Martinez, I. Matanovic and Y. S. Kim, *J. Phys. Chem. Lett.*, **7**, 4464 (2016).
45. J. H. Dumont, A. J. Spears, R. P. Hjelm, M. Hawley, S. Maurya, D. Li, G. Yuan, E. B. Watkins and Y. S. Kim, *ACS Appl. Mater. Interfaces*, **12**, 1825 (2020).
46. S. Maurya, J. H. Dumont, C. N. Villarrubia, I. Matanovic, D. Li, Y. S. Kim, S. Noh, J. Han, C. Bae, H. A. Miller, C. H. Fujimoto and D. R. Dekel, *ACS Catal.*, **8**, 9429 (2018).
47. I. Matanovic, H. T. Chung and Y. S. Kim, *J. Phys. Chem. Lett.*, **8**, 4918 (2017).
48. R. Zeng, Y. Yang, X. R. Feng, H. Q. Li, L. M. Gibbs, F. J. DiSalvo and H. D. Abruna, *Sci. Adv.*, **8** (2022).
49. D. M. Morales, M. A. Kazakova, S. Dieckhöfer, A. G. Selyutin, G. V. Golubtsov, W. Schuhmann and J. Masa, *Adv. Funct. Mater.*, **30**

(2019).
50. Y. Yang, H. Peng, Y. Xiong, Q. Li, J. Lu, L. Xiao, F. J. DiSalvo, L. Zhuang and H. D. Abruña, *ACS Energy Lett.*, **4**, 1251 (2019).
51. X. Chen, N. Wang, K. Shen, Y. Xie, Y. Tan and Y. Li, *ACS Appl. Mater. Interfaces*, **11**, 25976 (2019).
52. S. Lee, M. Choun, Y. Ye, J. Lee, Y. Mun, E. Kang, J. Hwang, Y. H. Lee, C. H. Shin, S. H. Moon, S. K. Kim, E. Lee and J. Lee, *Angew. Chem. Int. Ed. Eng.*, **54**, 9230 (2015).
53. L. Rebollar, S. Intikhab, J. D. Snyder and M. H. Tang, *J. Electrochem. Soc.*, **165**, J3209 (2018).
54. Q. Jia, E. Liu, L. Jiao, J. Li and S. Mukerjee, *Curr. Opin. Electrochem.*, **12**, 209 (2018).
55. X. Wang, Y. Zheng, W. Sheng, Z. J. Xu, M. Jaroniec and S.-Z. Qiao, *Mater. Today*, **36**, 125 (2020).
56. E. Liu, L. Jiao, J. Li, T. Stracensky, Q. Sun, S. Mukerjee and Q. Jia, *Energy Environ. Sci.*, **13**, 3064 (2020).
57. X. Tian, P. Zhao and W. Sheng, *Adv. Mater.*, **31**, e1808066 (2019).
58. Y. Qiu, X. Xie, W. Li and Y. Shao, *Chin. J. Catal.*, **42**, 2094 (2021).
59. R. Samanta, R. Mishra and S. Barman, *ACS Sust. Chem. Eng.*, **10**, 3704 (2022).
60. S. Watzele, J. Fichtner, B. Garlyyev, J. N. Schwämmlein and A. S. Bandarenka, *ACS Catal.*, **8**, 9456 (2018).
61. F. Song, T. Zhang, Y. Qian, J. Shaw, S. Chen, G. Chen, Y. Sun and Y. Rao, *Mater. Today Energy*, **22** (2021).
62. Y.-F. Xing, Y. Zhou, Y.-B. Sun, C. Chi, Y. Shi, F.-B. Wang and X.-H. Xia, *J. Electroanal. Chem.*, **872** (2020).
63. L. Jiao, E. Liu, S. Hwang, S. Mukerjee and Q. Jia, *ACS Catal.*, **11**, 8165 (2021).
64. S. Zhu, X. Qin, Y. Yao and M. Shao, *J. Am. Chem. Soc.*, **142**, 8748 (2020).
65. X. Qin, S. Zhu, Y. Wang, D. Pan and M. Shao, *Electrochim. Acta*, **425** (2022).
66. X. Yang, J. Nash, N. Oliveira, Y. Yan and B. Xu, *Angew. Chem. Int. Ed. Eng.*, **58**, 17718 (2019).
67. S. A. Giles, J. C. Wilson, J. Nash, B. Xu, D. G. Vlachos and Y. Yan, *J. Catal.*, **367**, 328 (2018).
68. Y. Xue, L. Shi, X. Liu, J. Fang, X. Wang, B. P. Setzler, W. Zhu, Y. Yan and Z. Zhuang, *Nat. Commun.*, **11**, 5651 (2020).
69. S. Lu and Z. Zhuang, *J. Am. Chem. Soc.*, **139**, 5156 (2017).
70. D. Strmcnik, M. Uchimura, C. Wang, R. Subbaraman, N. Danilovic, D. van der Vliet, A. P. Paulikas, V. R. Stamenkovic and N. M. Markovic, *Nat. Chem.*, **5**, 300 (2013).
71. S. M. Alia, B. S. Pivovar and Y. Yan, *J. Am. Chem. Soc.*, **135**, 13473 (2013).
72. J. Ohyama, T. Sato, Y. Yamamoto, S. Arai and A. Satsuma, *J. Am. Chem. Soc.*, **135**, 8016 (2013).
73. J. Zheng, Z. Zhuang, B. Xu and Y. Yan, *ACS Catal.*, **5**, 4449 (2015).
74. M. E. Scofield, Y. Zhou, S. Yue, L. Wang, D. Su, X. Tong, M. B. Vukmirovic, R. R. Adzic and S. S. Wong, *ACS Catal.*, ***6***, 3895 (2016).
75. B. Qin, H. Yu, J. Chi, J. Jia, X. Gao, D. Yao, B. Yi and Z. Shao, *RSC Adv.*, **7**, 31574 (2017).
76. J. Jiang, S. Tao, Q. He, J. Wang, Y. Zhou, Z. Xie, W. Ding and Z. Wei, *J. Mater. Chem. A*, **8**, 10168 (2020).
77. M. Wang, H. Yang, J. Shi, Y. Chen, Y. Zhou, L. Wang, S. Di, X. Zhao, J. Zhong, T. Cheng, W. Zhou and Y. Li, *Angew. Chem. Int. Ed. Eng.*, **60**, 5771 (2021).
78. F. Song, W. Li, J. Yang, G. Han, P. Liao and Y. Sun, *Nat. Commun.*, **9**, 4531 (2018).
79. F. Yang, X. Bao, P. Li, X. Wang, G. Cheng, S. Chen and W. Luo, *Angew. Chem. Int. Ed. Eng.*, **58**, 14179 (2019).
80. R. Ma, G. Lin, Y. Zhou, Q. Liu, T. Zhang, G. Shan, M. Yang and J. Wang, *npj Comput. Mater.*, **5** (2019).
81. X. Ge, A. Sumboja, D. Wuu, T. An, B. Li, F. W. T. Goh, T. S. A. Hor, Y. Zong and Z. Liu, *ACS Catal.*, **5**, 4643 (2015).
82. B. B. Blizanac, P. N. Ross and N. M. Markovic, *Electrochim. Acta*, **52**, 2264 (2007).
83. N. Ramaswamy and S. Mukerjee, *J. Phys. Chem. C*, **115**, 18015 (2011).
84. N. Ramaswamy and S. Mukerjee, *Adv. Phys. Chem.*, **2012**, 1 (2012).
85. J. Suntivich, H. A. Gasteiger, N. Yabuuchi, H. Nakanishi, J. B. Goodenough and Y. Shao-Horn, *Nat. Chem.*, **3**, 546 (2011).
86. H. Osgood, S. V. Devaguptapu, H. Xu, J. Cho and G. Wu, *Nano Today*, **11**, 601 (2016).
87. Y. Wang, Y. Yang, S. Jia, X. Wang, K. Lyu, Y. Peng, H. Zheng, X. Wei, H. Ren, L. Xiao, J. Wang, D. A. Muller, H. D. Abruna, B. J. Hwang, J. Lu and L. Zhuang, *Nat. Commun.*, **10**, 1506 (2019).
88. J. Jo, J. M. Yoo, D. H. Mok, H. Y. Jang, J. Kim, W. Ko, K. Yeom, M. S. Bootharaju, S. Back, Y. E. Sung and T. Hyeon, *Nano Lett.*, **22**, 3636 (2022).
89. J. Kim, W. Ko, J. M. Yoo, V. K. Paidi, H. Y. Jang, M. Shepit, J. Lee, H. Chang, H. S. Lee, J. Jo, B. H. Kim, S. P. Cho, J. van Lierop, D. Kim, K. S. Lee, S. Back, Y. E. Sung and T. Hyeon, *Adv. Mater.*, **34**, e2107868 (2022).
90. M. Sharma, J.-H. Jang, D. Y. Shin, J. A. Kwon, D.-H. Lim, D. Choi, H. Sung, J. Jang, S.-Y. Lee, K. Y. Lee, H.-Y. Park, N. Jung and S. J. Yoo, *Energy Environ. Sci.*, **12**, 2200 (2019).
91. H. Singh, S. Zhuang, B. Ingis, B. B. Nunna and E. S. Lee, *Carbon*, **151**, 160 (2019).
92. D. Wang, P. Yang, L. Liu, W. Wang and Z. Chen, *Mater. Today Energy*, **26** (2022).
93. H. Xu, D. Wang, P. Yang, A. Liu, R. Li, Y. Li, L. Xiao, X. Ren, J. Zhang and M. An, *J. Mater. Chem. A*, **8**, 23187 (2020).
94. S. Park, M. Her, H. Shin, W. Hwang and Y.-E. Sung, *ACS Appl. Energy Mater.*, **4**, 1459 (2021).
95. A. Zitolo, V. Goellner, V. Armel, M. T. Sougrati, T. Mineva, L. Stievano, E. Fonda and F. Jaouen, *Nat. Mater.*, **14**, 937 (2015).
96. Y. J. Sa, D. J. Seo, J. Woo, J. T. Lim, J. Y. Cheon, S. Y. Yang, J. M. Lee, D. Kang, T. J. Shin, H. S. Shin, H. Y. Jeong, C. S. Kim, M. G. Kim, T. Y. Kim and S. H. Joo, *J. Am. Chem. Soc.*, **138**, 15046 (2016).
97. S. H. Lee, J. Kim, D. Y. Chung, J. M. Yoo, H. S. Lee, M. J. Kim, B. S. Mun, S. G. Kwon, Y. E. Sung and T. Hyeon, *J. Am. Chem. Soc.*, **141**, 2035 (2019).
98. K. Im, K. H. Choi, B. J. Park, S. J. Yoo and J. Kim, *Energy Conv. Manag.*, **265** (2022).
99. J. Lee, H. S. Kim, J.-H. Jang, E.-H. Lee, H.-W. Jeong, K.-S. Lee, P. Kim and S. J. Yoo, *ACS Sust. Chem. Eng.*, **9**, 7863 (2021).
100. H. S. Kim, C. H. Lee, J.-H. Jang, M. S. Kang, H. Jin, K.-S. Lee, S. U. Lee, S. J. Yoo and W. C. Yoo, *J. Mater. Chem. A*, **9**, 4297 (2021).
101. E. Proietti, F. Jaouen, M. Lefevre, N. Larouche, J. Tian, J. Herranz and J. P. Dodelet, *Nat. Commun.*, **2**, 416 (2011).
102. H. Zhang, S. Hwang, M. Wang, Z. Feng, S. Karakalos, L. Luo, Z. Qiao, X. Xie, C. Wang, D. Su, Y. Shao and G. Wu, *J. Am. Chem.*

Soc., **139**, 14143 (2017).
103. Y. Chen, S. Ji, Y. Wang, J. Dong, W. Chen, Z. Li, R. Shen, L. Zheng, Z. Zhuang, D. Wang and Y. Li, *Angew. Chem. Int. Ed. Eng.*, **56**, 6937 (2017).
104. G.-S. Kang, J.-H. Jang, S.-Y. Son, Y.-K. Lee, D. C. Lee, S. J. Yoo, S. Lee and H.-I. Joh, *J. Power Sources*, **520** (2022).
105. J. Y. Jung, S. Kim, J.-G. Kim, M. J. Kim, K.-S. Lee, Y.-E. Sung, P. Kim, S. J. Yoo, H.-K. Lim and N. D. Kim, *Nano Energy*, **97** (2022).

Sung Jong Yoo obtained his Ph.D. degree from the School of Chemical and Biological Engineering at Seoul National University in 2009 and moved to KIST (Korea Institute of Science and Technology) for postdoctoral research. He began his independent career in 2012 as senior research scientist in the Fuel Cell Research Center at KIST. He is currently a principal scientist at Center for Hydrogen & Fuel Cell Research of KIST. His current research interests include: (i) the influence of surface chemistry of metal nanoparticles on catalytic activities and stability, (ii) the design principles for oxygen reduction activity on oxide catalysts for fuel cells, and (iii) the catalytic activity trends of oxygen reduction reaction for alkaline anion exchange membrane fuel cell.